SI Methods

All analysis code for the novel metrics introduced below, along with tutorials, is available at https://github.com/voytekresearch/misshapen. Phase-amplitude coupling was calculated using the open-source pacpy package, available at https://github.com/voytekresearch/pacpy.

Data collection
M1 recordings were obtained from 23 PD patients and 9 dystonia patients as previously described (1–3). PD and cervical dystonia patients were recruited at the University of California at San Francisco (UCSF) or the San Francisco Veteran Affairs Medical Center. PD patients were diagnosed with idiopathic PD with mild to moderate bradykinesia/rigidity and UPDRS III (Unified Parkinson's Disease Rating Scale part III) scores between 30 and 60. Patients underwent DBS implantation in the awake state and provided written informed consent. Patients were excluded if they had prominent tremor or peak-to-peak M1 LFP amplitude below 50 microvolts. Data collection was approved by the institutional ethics committees and was in agreement with the Declaration of Helsinki.

Deep Brain Stimulation (DBS) was as previously described (2). T2-weighted magnetic resonance imaging was used to target the STN, with adjustments made based on movement-related spiking activity. Intraoperative computed tomography scans coregistered with preoperative MRI were used to confirm electrode placement of the DBS lead (model 3389 in 17 patients and 3387 in 6 patients; Medtronic, Inc., Minneapolis, Minnesota, USA). An analog neurostimulator (Medtronic model 3625) was used to set therapeutic stimulation parameters. Because optimal stimulation settings were not found prior to recording, an increased voltage (4V) was used for stimulation between the motor territory of STN and its dorsal border. More details on patients and stimulation can be found in the previous reports (1, 2).

A six-contact subdural electrocorticography (ECoG) strip was placed on the cortical surface using the burr hole for DBS lead placement. The target was the arm area of M1, 3cm from midline and medial to the hand knob. Electrode contacts were platinum with a 4mm total diameter, 2.3mm exposed diameter, and 1cm spacing between contacts (Ad-Tech, Racine, WI). Correct placement of electrodes was confirmed using intraoperative computed tomography (iCT) merged with preoperative MRI or lateral fluoroscopy. Additionally, physiological confirmation was obtained using median nerve stimulation (frequency = 2 Hz, pulse width = 200 μs, pulse train length = 160, amplitude = 25–40 mAmp) to evoke somatosensory potentials. The most posterior contact showing a negative N20 waveform was defined as the closest electrode to M1.

Antiparkinsonian and antidystonic medication was stopped 12 hours before surgery. Data were collected 5-60 minutes after lead insertion to minimize the confounding effect of a temporary 'microlesion' associated with lead insertion. In bilateral DBS implantation surgeries, brain activity was recorded on the second side implanted in order to allow more time between the cessation of propofol sedation and the start of ECoG recording. First, 'pre-DBS' (or 'DBS off') data were collected and evaluated after lead insertion, before any stimulation. Second, 'DBS on' data were

collected when DBS was turned on for the first time, before searching for optimal contact and stimulation parameters. Third, 'after DBS' data were collected after DBS turned off for several minutes.

Recordings were collected using Alpha Omega Microguide Pro (Alpha Omega, Inc, Nazareth, Israel) or the Guideline 4000 customized clinical recording system (FHC Inc, Bowdoin, ME) with a sampling rate between 1000 Hz and 3000 Hz. The five most posterior contacts (C1-5) were referenced to the most anterior one (C6). A needle electrode in the scalp was used as the ground. Signals were band-pass filtered 1–500 Hz and amplified 7000x. While the analyzed data was collected, subjects were relaxing with eyes open, fixating on a point approximately 1 meter away. The first 30 seconds of data without obvious electrical noise or movement were selected for analyses.

Data pre-processing

Recordings were referenced using a bipolar montage in which each channel was referenced to the immediately anterior channel (i.e. C1–C2, C2–C3, etc.). Data were downsampled to 1000 Hz. Line noise was removed with a notch filter between 58 Hz and 62 Hz (Butterworth, order 3). Additionally, all signals were cleaned of high frequency artifacts by applying narrowband notch filters (Butterworth, order 3) to remove any sharp peaks in power spectra above 80 Hz caused by DBS stimulation and electronic noise. The same filters were applied to all recordings from the same subject (pre-DBS, during, and post-DBS).

Oscillation sharpness

The first step in quantifying the sharpness of the beta oscillations was to identify the time points of peaks and troughs. First, the raw voltage trace was band-pass filtered using an FIR filter with cutoff frequencies at 13 Hz and 30 Hz and a filter length of 231 ms (3 cycles at 13Hz). Time points of rising and falling zero-crossings were identified. Returning to the raw signal, the time point of maximal voltage between a rising zero-crossing and a subsequent falling zero-crossing was defined as the peak. Similarly, the time point of minimal voltage between a falling zero-crossing and a subsequent rising zero-crossing was defined as a trough.

Sharpness of each peak and trough was defined by calculating the average of the absolute voltage change 5 ms preceding and following the extrema, as in the equation below.

$$Sharpness_{peak} = \frac{(V_{peak} - V_{peak-5ms}) + (V_{peak} - V_{peak+5ms})}{2}$$

Trough sharpness was calculated in the same way. The higher the absolute voltage difference between the extrema and these surrounding time points, the sharper the peak. While 5 ms was chosen as the temporal width to quantify sharpness, results were similar for other choices of sharpness width (see Fig. S9).

The average sharpness throughout a recording was calculated for peaks and troughs separately (typically about 600 each in a 30 second recording). The reported extrema sharpness ratio (ESR) metric was calculated by calculating the ratio of the sharpness of the two extrema, such that the ratio is always greater than 1 (see equation below). This ratio accounts for differences in the amplitudes across subjects that can be caused by variance in electrode conductance.

$$ESR = max(\frac{Sharpness_{peaks}}{Sharpness_{troughs}}, \frac{Sharpness_{troughs}}{Sharpness_{peaks}})$$

Note in Figure 2, this ratio is not fixed to be greater than 1, but rather peak sharpness is divided by trough sharpness.

Oscillation steepness

Steepness of the rise and decays of each oscillation was calculated by taking advantage of the peaks and troughs identified as described above. For rise steepness, the time series of interest was the raw voltage between each trough and the subsequent peak. The maximum value of the instantaneous first derivative of this signal was defined as the steepness for this single rise period. The steepness of decay periods were similarly calculated using the raw voltage time series between each peak and the subsequent trough. A rise-decay steepness ratio (RDSR) was then calculated for each recording by dividing the average steepness for all rises by the average steepness for all decays.

$$RDSR = max(\frac{Steepness_{decays}}{Steepness_{rises}}, \frac{Steepness_{rises}}{Steepness_{decays}})$$

Note in Figure 2, this ratio is not fixed to be greater than 1, but rather rise steepness is divided by decay steepness.

Spectral analysis

High gamma amplitude (Fig. 4B,D) was calculated by band-pass filtering signals (50-200Hz, FIR filter, length = 60ms) and subsequently calculating the magnitude of its Hilbert transform. The high gamma amplitude was sampled at the time of extrema voltage in each oscillation (Fig. 3C and Fig. S4A,B) or the time of greatest voltage change in each oscillatory rise and decay (Fig. S1E and Fig. S4C,D). The peak- and trough-locked high gamma amplitude (Fig. 3D and Fig. S5) was calculated using the extrema found as above. The extrema were split into two equal groups based on the sharpness calculated as above.

Beta and high gamma power (Fig. S8) were calculated for each 30-second signal by summing the raw power spectrum in their respective frequency ranges (13-30 Hz and 50-200 Hz). The raw power spectrum was calculated by taking the absolute value of the square of the raw FFT (numpy.fft.fft).

Phase-amplitude coupling (PAC) was calculated using the normalized modulation index metric (4). Each subject's recording was band-pass filtered with a finite-impulse response (FIR) filter with length equal to 3 cycles of the low cutoff frequency. The high gamma amplitude was calculated as described above in this section. The beta phase was similarly calculated by band-pass filtering between 13-30 Hz and calculating the angle of the Hilbert-transform of the signal. While a normalized modulation index (4) was first applied to quantify PAC, results were similar when applying four additional metrics of PAC (Fig. S10) (5–7), or when a comodulogram method was used as in the previous report (2).

Comodulograms (Fig. 4C,E and Fig. 3A) were calculated similar to the previous report (2). The frequency range for the phase-providing oscillation ranged from 6 Hz to 40 Hz with a step size and bandwidth of 2Hz. For the amplitude-providing oscillation, the frequency ranged from 20 Hz to 200 Hz with a step size and bandwidth of 4 Hz. The modulation index method (6) was used to quantify PAC between each combination of signals.

Phase-amplitude coupling histograms (Fig. 5D and Fig. S3) were calculated from the beta phase time series and high gamma amplitude time series used to calculate PAC. The high gamma amplitude was then averaged across 10 equally-sized beta phase bins.

Waveform phase estimate

A similar phase estimate as described previously (8–10) was applied to estimate the instantaneous phase in this data set (Fig. S11). Time points of peaks and troughs were identified as in the "Oscillation Sharpness" section above. The time points of these extrema were then used to linearly interpolate a theoretical phase value for each sample. This phase estimate was used only to visually display that the high gamma amplitude is specifically coupled to the beta peaks and troughs (Fig. S3).

Simulated neuronal synchrony and LFP

Methodology for simulation of point neurons and their associated LFP is illustrated in Fig. S12. A population of 100 point neurons were simulated with synaptic events controlled by a non-homogenous Poisson process, as Parkinsonian basal ganglia firing is reasonably approximated by a Poisson interspike interval distribution (11, 12). The rate of synaptic events was biased by a beta oscillation, simulated by filtering white noise with a band-pass FIR filter with cutoff frequencies of 13 and 30 Hz. This rate was mapped to the phase of the beta oscillation with a Gaussian function centered at 0 radians and a standard deviation of 0.5 radians for the high synchrony case and 1.0 radians for the low synchrony case. Synaptic event rate was fixed to be 30 Hz. 50% of the synaptic event rate was biased by the simulated beta phase, and the other 50% was phase-independent. Additionally, 50% of neurons produced synaptic events completely independent of beta phase. Population firing was simulated for 5 seconds with a 1kHz sampling rate. LFPs were simulated by convolving the time series of population synaptic events with an empirically estimated AMPA synaptic current (double-exponential, 0.3 ms rise time constant, 2 ms decay time constant) (13). Oscillation sharpness and PAC were then estimated on the simulated LFPs using the methods described above.

A canonical signal with beta-high gamma phase-amplitude coupling (Fig. 4D) was simulated in three steps: 1. A beta oscillation was simulated by band-pass filtering 30 seconds of white noise with a band-pass FIR filter (13-30 Hz). 2. High gamma was similarly simulated by band-pass filtering 30 seconds of white noise with a 50-200 Hz band-pass FIR filter. The amplitude of the high gamma was then biased by the beta phase by multiplying the time series by $(1 - abs(\phi_\beta)/\pi)$ and scaled by 0.02 in order to decrease its amplitude relative to the simulated beta oscillation. 3. The beta oscillation and high gamma components were added together.

Statistics

The Scipy package (v 0.16.0) in Python (v 2.7) was used for all statistical analysis including unpaired and paired *t*-tests, Mann-Whitney U tests, Pearson correlations, and Spearman correlations.

References

1. de Hemptinne C, et al. (2013) Exaggerated phase-amplitude coupling in the primary motor cortex in Parkinson disease. *Proc Natl Acad Sci U S A* 110(12):4780–5.
2. de Hemptinne C, et al. (2015) Therapeutic deep brain stimulation reduces cortical phase-amplitude coupling in Parkinson's disease. *Nat Neurosci* 18(5):779–786.
3. Panov F, et al. (2016) Intraoperative electrocorticography for physiological research in movement disorders: principles and experience in 200 cases. *J Neurosurg*:1–10.
4. Ozkurt TE, Schnitzler A (2011) A critical note on the definition of phase-amplitude cross-frequency coupling. *J Neurosci Methods* 201(2):438–443.
5. Canolty RT, et al. (2006) High Gamma Power is Phase-Locked to Theta Oscillations in Human Neocortex. 313(5793):1626–1628.
6. Tort ABL, Komorowski R, Eichenbaum H, Kopell N (2010) Measuring Phase-Amplitude Coupling Between Neuronal Oscillations of Different Frequencies. *J Neurophysiol* 104(2):1195–1210.
7. Penny WD, Duzel E, Miller KJ, Ojemann JG (2008) Testing for nested oscillation. *J Neurosci Methods* 174(1):50–61.
8. Siapas AG, Lubenov E V., Wilson MA (2005) Prefrontal phase locking to hippocampal theta oscillations. *Neuron* 46(1):141–151.
9. Belluscio M a., Mizuseki K, Schmidt R, Kempter R, Buzsaki G (2012) Cross-Frequency Phase-Phase Coupling between Theta and Gamma Oscillations in the Hippocampus. *J Neurosci* 32(2):423–435.
10. Trimper JB, Stefanescu RA, Manns JR (2014) Recognition memory and theta-gamma interactions in the hippocampus. *Hippocampus* 24(3):341–353.
11. Hutchison WD, et al. (1994) Differential neuronal activity in segments of globus pallidus in Parkinson's disease patients. *Neuroreport* 5(0959-4965 (Print)):1533–1537.
12. Mallet N, et al. (2008) Parkinsonian beta oscillations in the external globus pallidus and their relationship with subthalamic nucleus activity. *J Neurosci* 28(52):14245–14258.
13. Angulo MC, Rossier J, Audinat E (1999) Postsynaptic glutamate receptors and integrative properties of fast-spiking interneurons in the rat neocortex. *J Neurophysiol* 82(3):1295–1302.

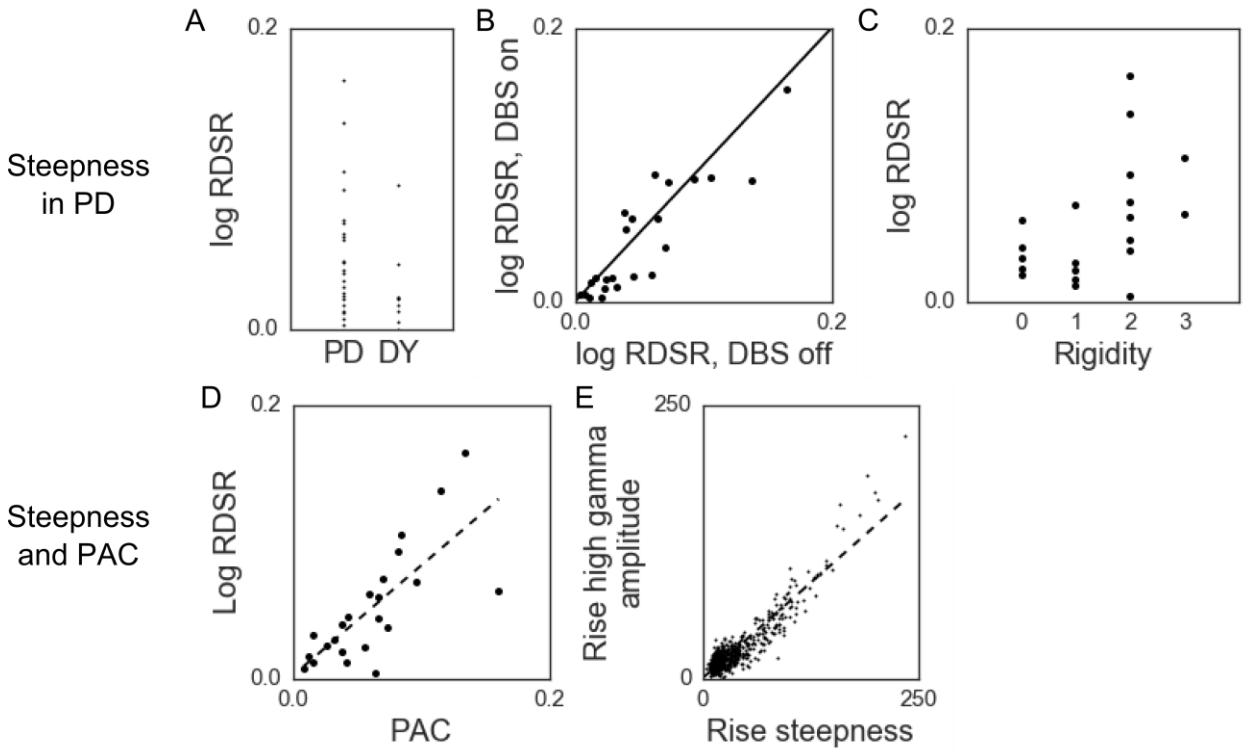

Figure S1. Oscillatory rise-decay steepness ratio (RDSR) in Parkinson's Disease and its relationship to PAC. Note these results are similar but milder compared to those obtained with ESR. (A) There is a trend of higher RDSR in PD patients compared to cervical dystonia patients (Mann-Whitney U test, $U_{30} = 59$, $p = 0.13$). (B) There is a trend of decreased RDSR in PD patients with DBS application (paired t-test, $t_{22} = 1.6$, $p = 0.12$). (C) The clinical rigidity score pre-DBS is positively correlated with RDSR (Spearman $r = 0.52$; $n = 23$; $p = 0.018$). (D) RDSR is strongly correlated with PAC ($r = 0.75$; $p < 10^{-4}$). (E) Rise steepness is highly correlated with the high gamma amplitude at that time ($r = 0.92$; $p < 10^{-251}$) shown for one exemplar PD patient pre-DBS.

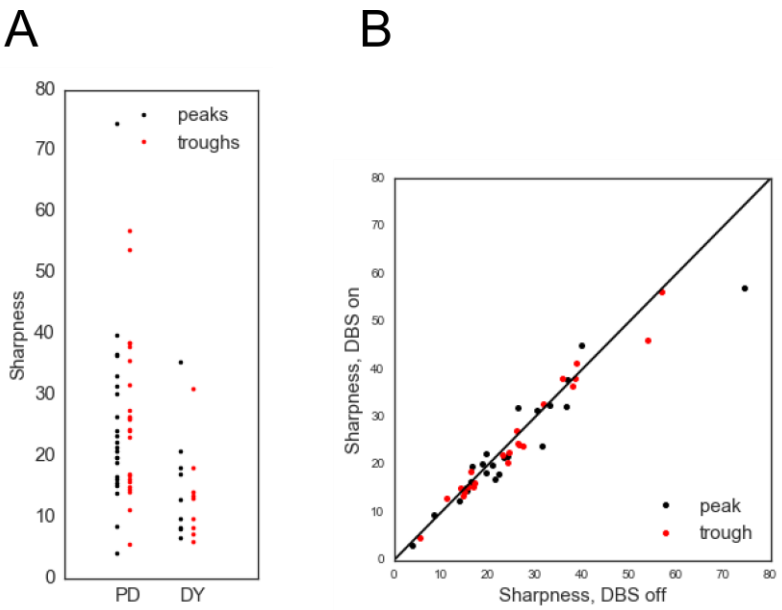

Figure S2. Peak and trough sharpness is increased in untreated PD. (A) PD patients have significantly sharper extrema than cervical dystonia (DY) patients (Mann-Whitney *U* test, U_{62} = 171, p = 0.0003). (B) DBS decreases the sharpness of peaks and troughs (paired *t*-test, t_{45} = 1.8, p = 0.071). Each dot represents 1 subject. Solid line represents unity.

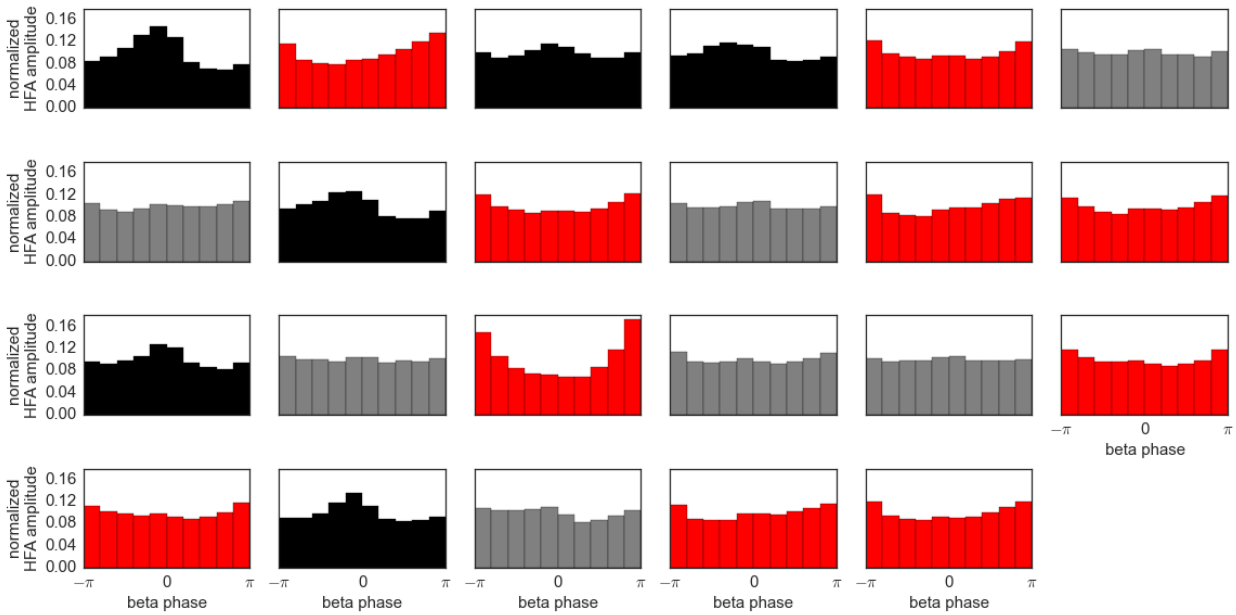

Figure S3. Distributions of high gamma amplitude as a function of beta phase. Each subplot represents the recording from 1 PD patient pre-DBS. Notice that PAC predominantly occurs at the peak (black) or trough (red), while gray distributions show no obvious PAC.

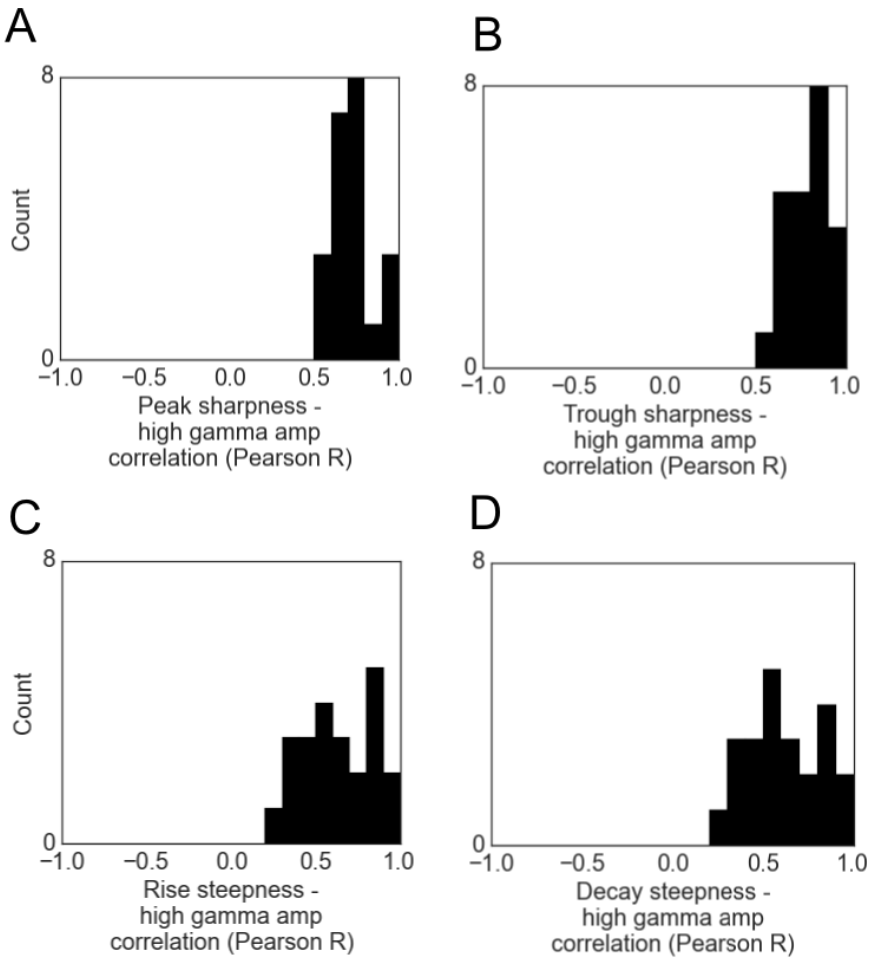

Figure S4. Histograms for Pearson correlation coefficients between shape metrics and high gamma amplitude. For all subjects, peak instantaneous high gamma amplitude is positively correlated with (A) peak sharpness, (B) trough sharpness, (C) rise steepness, and (D) decay steepness. Each count is calculated from the recording of a PD patient pre-DBS.

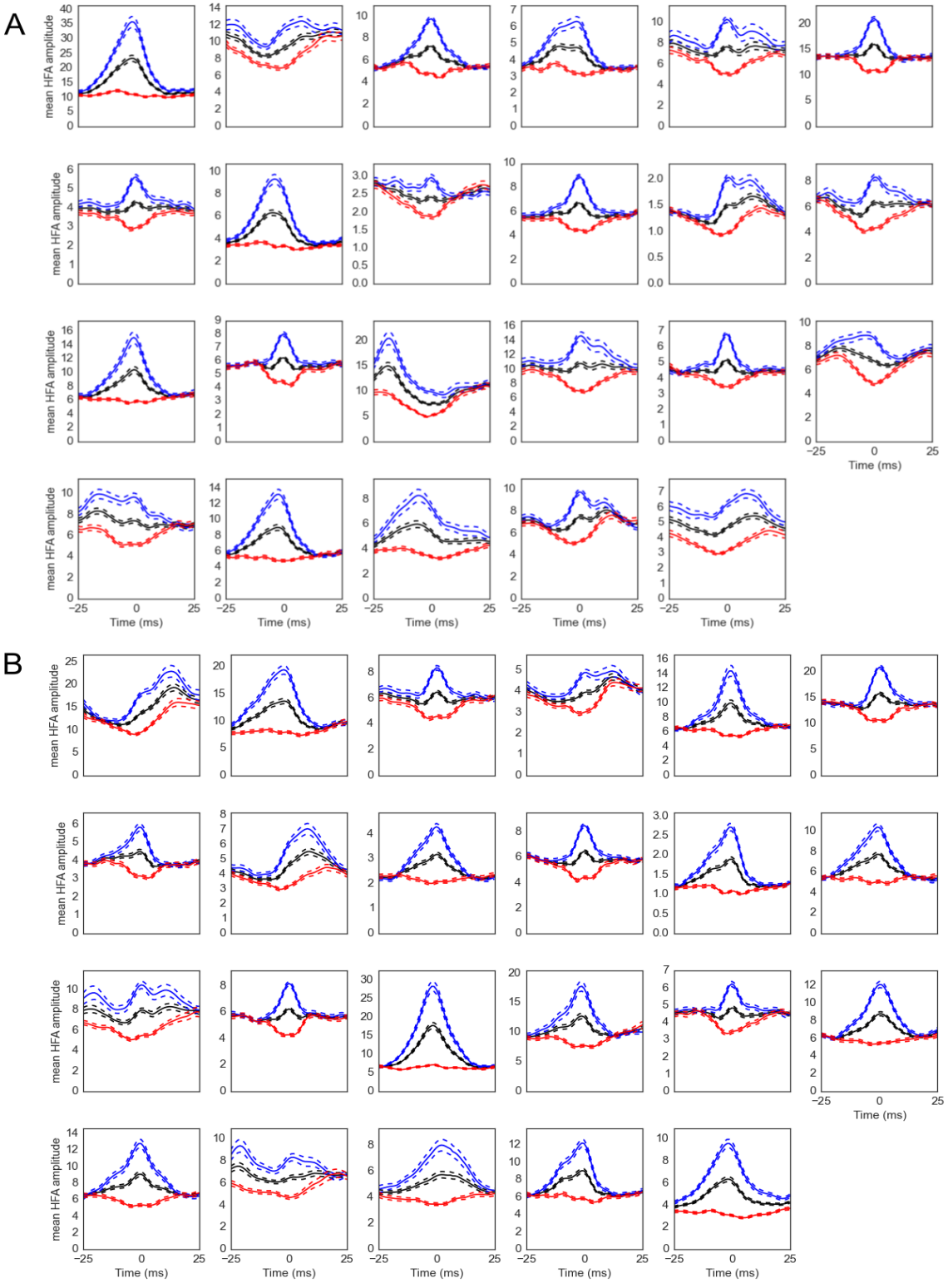
A
B
mean HFA amplitude
Time (ms)
−25
0
25

Figure S5. High gamma amplitude is time-locked to sharp oscillatory (A) peaks and (B) troughs. The same color scheme from Fig. 3D applies (black: all extrema, blue: sharpest 50% of extrema, red: flattest 50% of extrema). Each subplot represents the recording from 1 PD patient pre-DBS. Note that each patient possesses increased high gamma amplitude locked to the peak and/or trough, and that this locking is dependent on the sharpness of the extrema. Solid lines denote mean and dashed lines denote SEM.

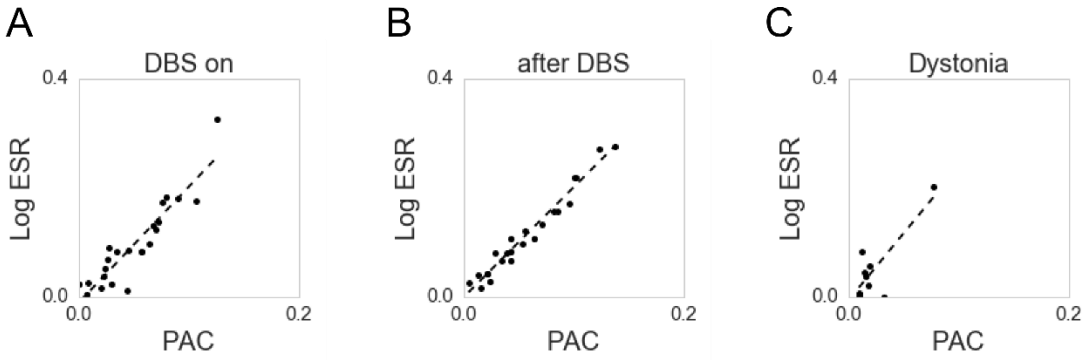

Figure S6. ESR-PAC correlation holds for all groups of subjects. PD patients pre-DBS were shown in Fig. 3B. ESR-PAC is also strongly correlated for PD patients (A) on DBS ($r = 0.92$, $p < 10^{-9}$) and (B) post-DBS ($r = 0.82$, $p < 10^{-15}$) as well as (C) cervical dystonia patients ($r = 0.82$, $p < 10^{-3}$).

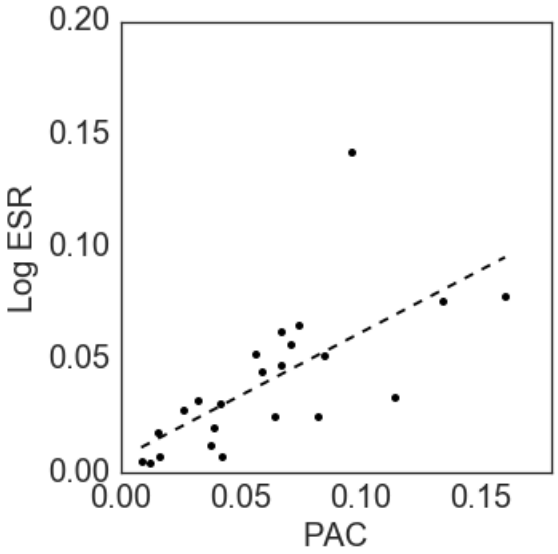

Figure S7. The correlation between ESR and PAC is robust when sharpness is calculated on low-pass-filtered data (FIR, filter order = 60 ms, cutoff frequency = 50 Hz) such that negligible high gamma remains in the signal (>50 dB attenuation).

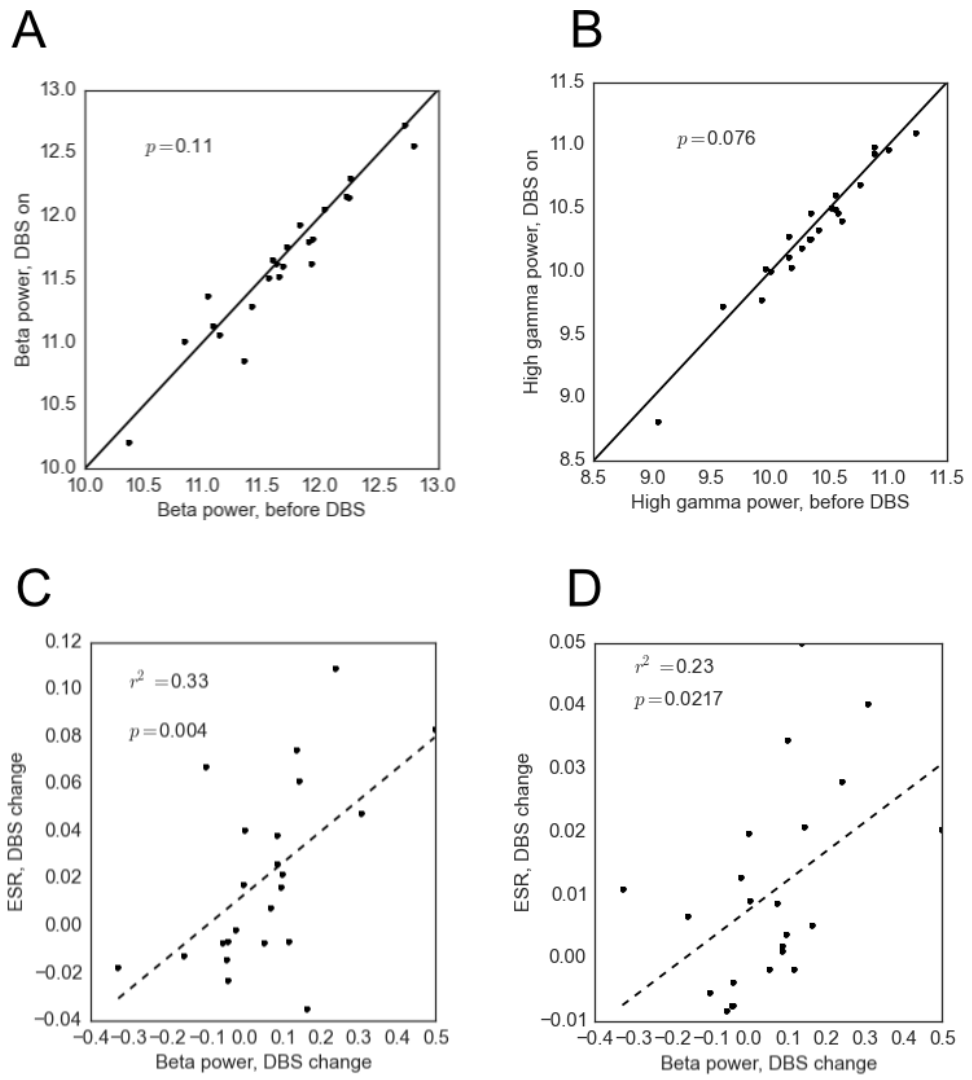

Figure S8. Beta and high gamma power effects with DBS. Beta power (A) and high gamma power (B) have trending decreases with DBS (solid lines represent unity). Paired t-tests were performed to obtain the *p*-values shown. (C) DBS-induced beta power change is positively correlated with ESR change (D) and PAC change. Each dot represents one PD patient. Correlation coefficients are Pearson.

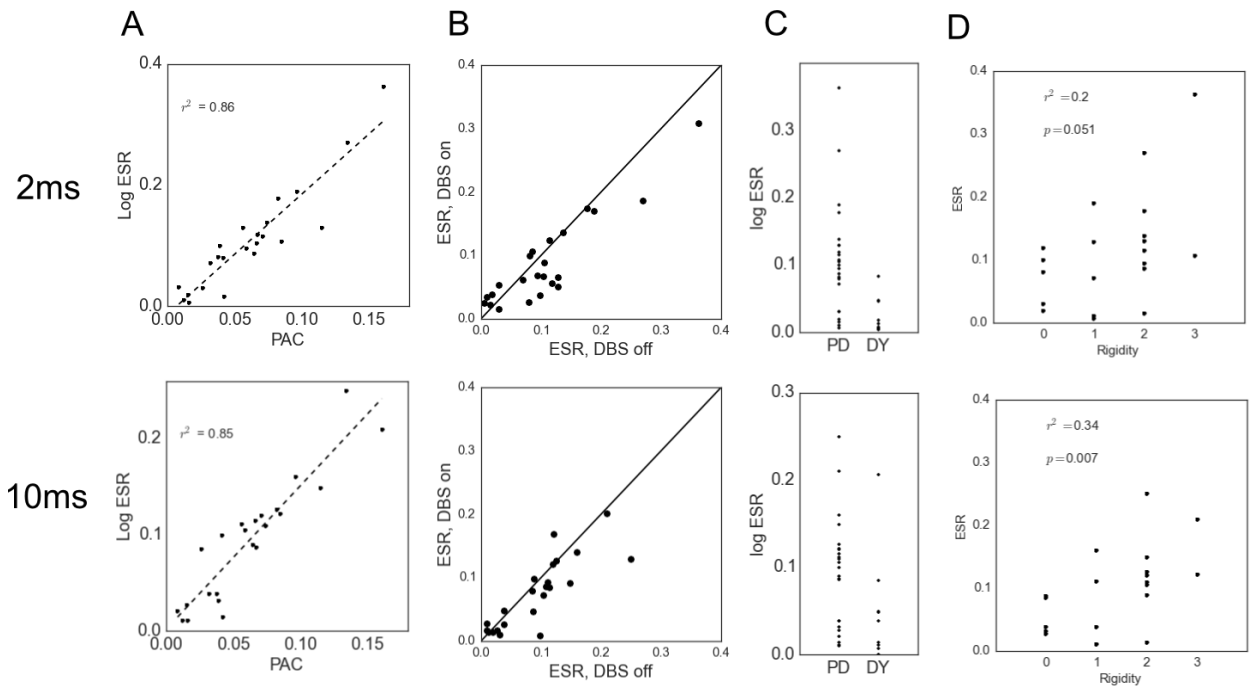

Figure S9. Results of oscillation sharpness analysis hold at various temporal scales. (A) PAC and ESR are highly correlated using a time window of calculating sharpness of 2 ms (top, r = 0.93, $p < 10^{-9}$) or 10 ms (bottom, r = 0.92, $p < 10^{-9}$). (B) ESR decreases with DBS application when applying a time window of calculating sharpness of 2 ms (top, paired t-test, t_{22} = 2.7, p = 0.014) or 10 ms (bottom, paired t-test, t_{22} = 2.5, p = 0.022) (solid lines represent unity).(C) ESR is higher in PD subjects compared to dystonia (DY) subjects when applying a time window of calculating sharpness of 2 ms (top, Mann-Whitney U test, U_{30} = 40, p = 0.008) or 10 ms (bottom, Mann-Whitney U test, U_{30} = 54, p = 0.040). (D) ESR and clinical rigidity scores are positively correlated when applying a time window of calculating sharpness of 2 ms (top, Spearman correlation, r = 0.44, p = 0.051) or 10 ms (bottom, Spearman correlation, r = 0.59, p = 0.007).

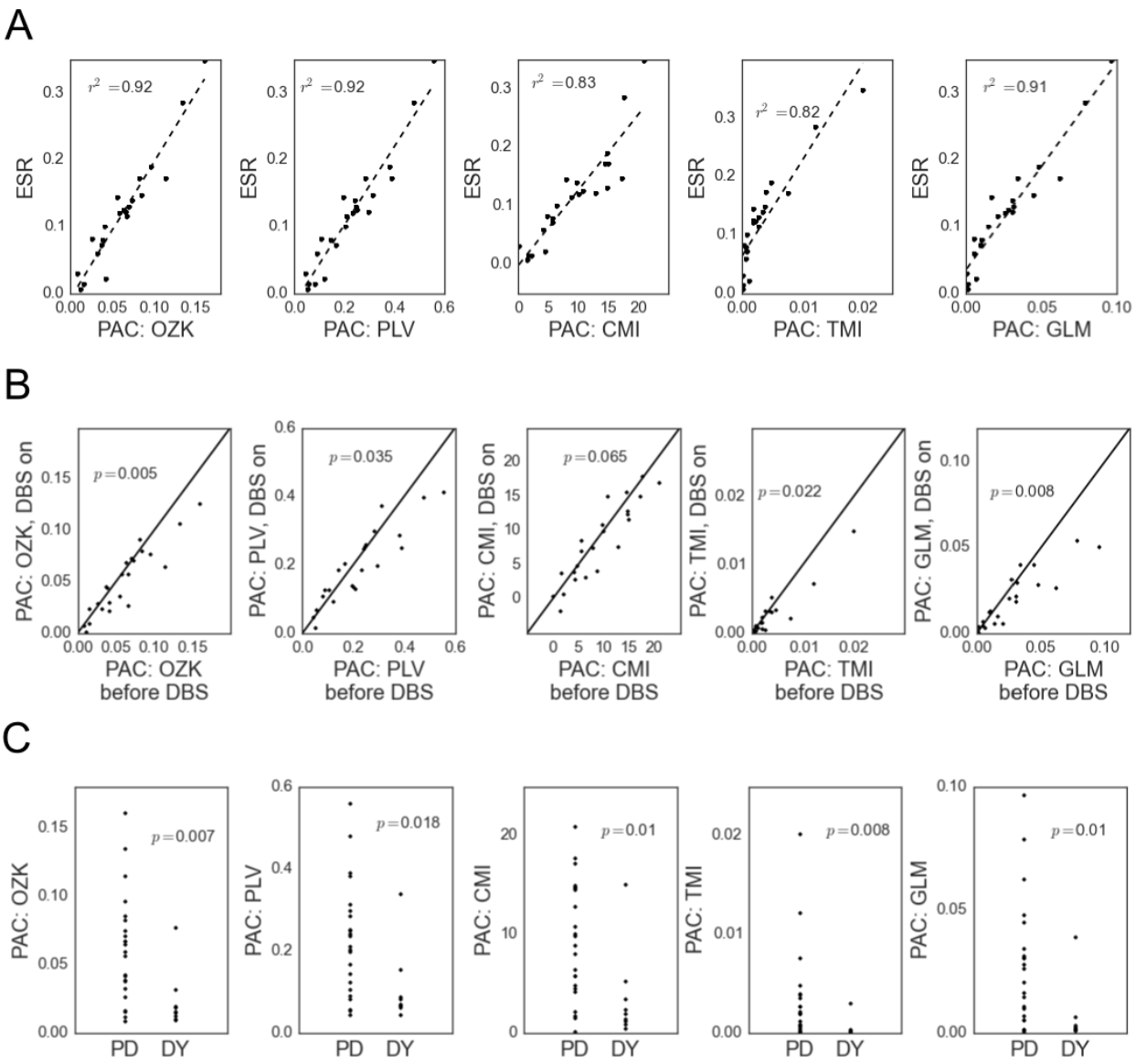

Figure S10. Results are unchanged by changing PAC calculation method for (A) PAC-ESR correlation, (B) PAC decrease with DBS, and (C) PAC greater in PD than dystonia. OZK = amplitude-normalized modulation index PAC estimate (4). PLV = phase-locking value PAC estimate (7). CMI = Canolty's modulation index PAC estimate (5). TMI = Tort's modulation index PAC estimate (6). GLM = general linear model PAC estimate (7). Correlation coefficients are Pearson. Paired *t*-tests were run to obtain the *p*-values in (B), and unpaired *t*-tests were run to obtain the *p*-values in (C).

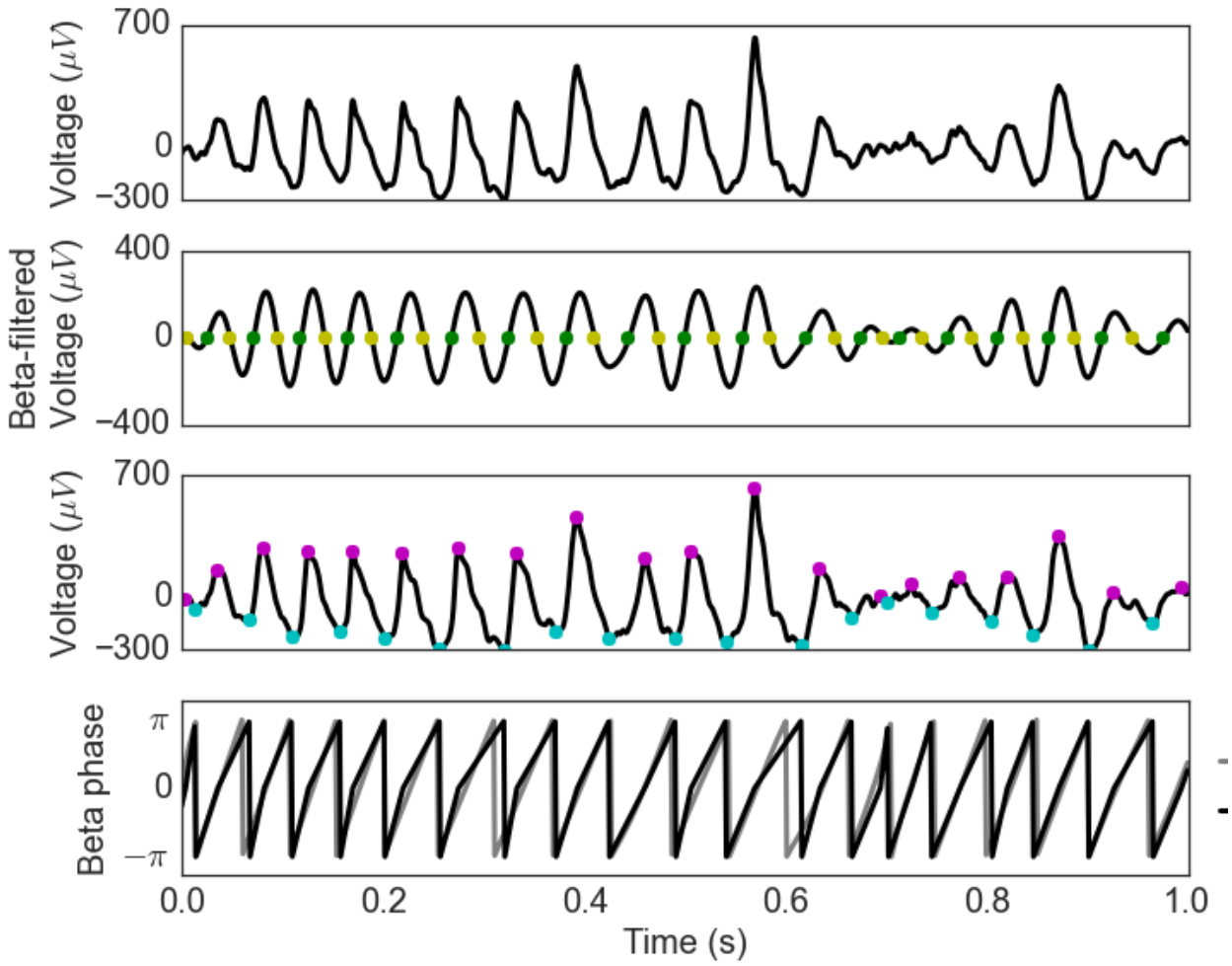

Figure S11. Methodology for identifying peaks and troughs, and calculating an instantaneous phase estimate. Raw voltage (row 1). Zero-crossings are identified in a signal band-pass filtered in the beta range (row 2). Green dots correspond to rising zero-crossings and yellow dots correspond to falling zero-crossings. Peaks and troughs are then identified by finding the time points of maximal and minimal voltage between each extrema (row 3). Pink dots correspond to peaks and blue dots correspond to troughs. Instantaneous phase is found by linear interpolation over time between peaks (phase = 0) and troughs (phase = -π,π) shown in black (row 4). This is compared to the result of the typical phase-estimation method of calculating the angle of the Hilbert transform of the band-pass filtered signal (gray).

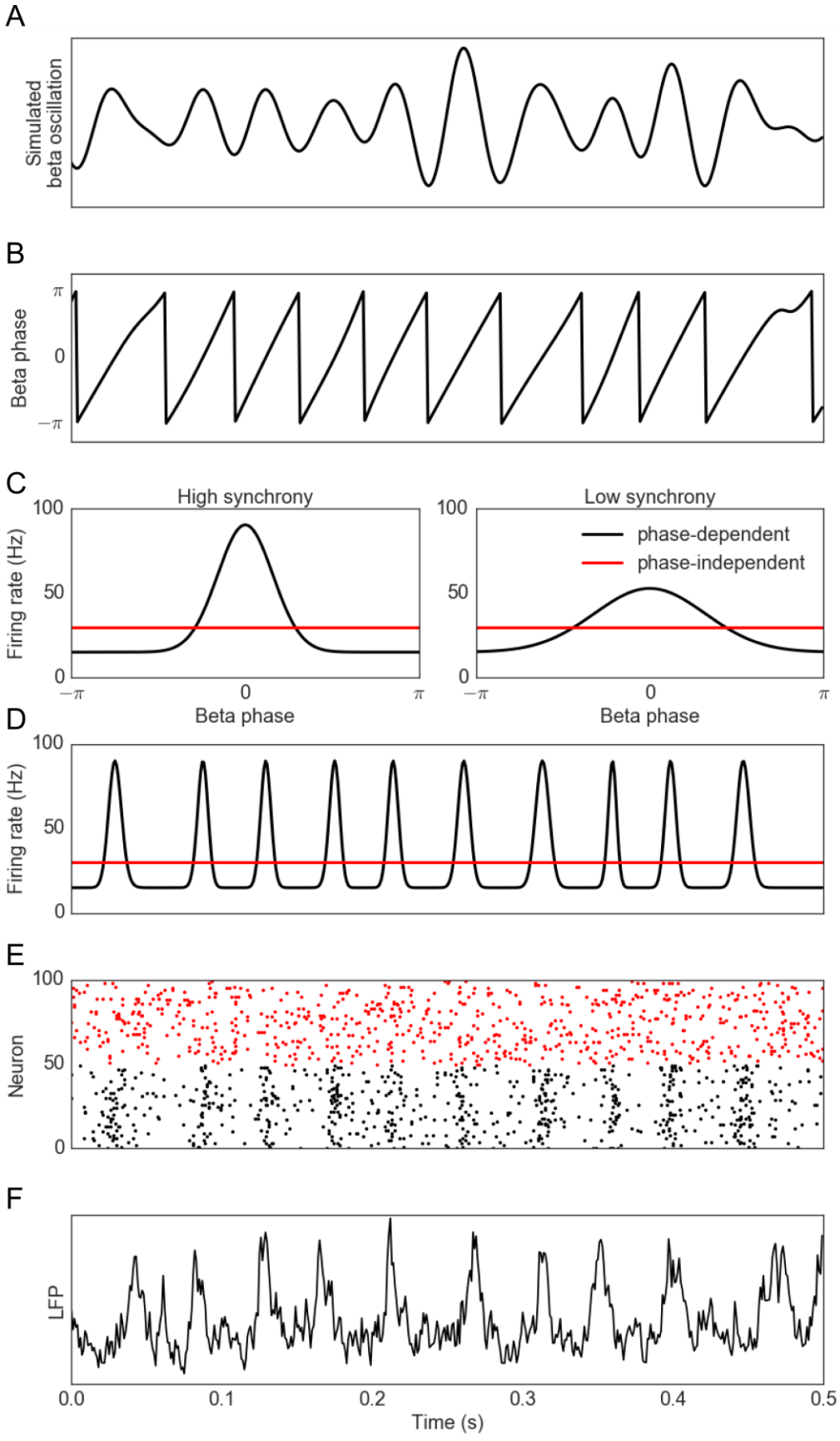
A
Simulated beta oscillation
B
Beta phase
π
0
−π
C
High synchrony
Low synchrony
phase-dependent
phase-independent
Firing rate (Hz)
100
50
0
−π
0
π
Beta phase
D
Firing rate (Hz)
E
Neuron
F
LFP
0.0
0.1
0.2
0.3
0.4
0.5
Time (s)

Figure S12. Method for simulating synchronous synaptic events. (A) White noise was filtered between 13 and 30 Hz to generate a beta oscillation. (B) The phase of the simulated beta oscillation. (C) The transform from phase to synaptic event rate for the high synchrony condition (left) and low synchrony condition (right). The black lines correspond to the neurons that have phase-biased synaptic events, and the red lines correspond to the neurons that have phase-independent synaptic events. The total synaptic event rate (area under the Gaussian) is equal in all cases, but the phase-specificity is altered. (D) The time-varying synaptic event rate. This was generated from the simulated phase in B and the high synchrony transform in C. Note that the average rate is equal for both neurons that are phase-dependent and phase-independent. (E) Raster of synaptic events generated by a Poisson process governed by the time-varying firing rates in D. (F) LFP simulated by convolving an AMPA synaptic current kernel with the time series of the synaptic events of all neurons in panel E. Note the sharp beta oscillation.